J Mater Sci (2022) 57:10997–11012

Chemical routes to materials

Synthesis and characterization of 2,5-furandicarboxylic acid poly(butanediol sebacate-butanediol) terephthalate (PBSeT) segment copolyesters with excellent water vapor barrier and good mechanical properties

Yu Feng[1], Yingchun Li[1,*], Xinming Ye[1], Zhimao Li[1], Wensheng Wang[1], Tong Liu[1], Islam H. El Azab[2], Gaber A. M. Mersal[3], Mohamed M. Ibrahim[3], Zeinhom M. El-Bahy[4], Mina Huang[5,6], and Zhanhu Guo[5,*]

[1] School of Materials Science and Engineering, North University of China, Taiyuan 030051, China
[2] Department of Food Science and Nutrition, College of Science, Taif University, P.O. Box 11099, Taif 21944, Saudi Arabia
[3] Department of Chemistry, College of Science, Taif University, P.O. Box 11099, Taif 21944, Saudi Arabia
[4] Department of Chemistry, Faculty of Science, Al-Azhar University, Nasr City, Cairo 11884, Egypt
[5] Integrated Composites Laboratory (ICL), Department of Chemical and Biomolecular Engineering, University of Tennessee, Knoxville, TN 37996, USA
[6] College of Materials Science and Engineering, Taiyuan University of Science and Technology, Taiyuan 030024, Shanxi, China

Received: 27 March 2022
Accepted: 23 April 2022
Published online: 12 May 2022

ABSTRACT

In order to improve the performance of biodegradable materials, aliphatic–aromatic copolyesters were synthesized from sebacic acid, terephthalic acid, 1,4-butanediol and 2,5-furandicarboxylic acid via two-step esterification and polycondensation. Copolyesters were characterized by intrinsic viscosity, gel permeation chromatography, X-ray diffraction, Fourier infrared spectroscopy, nuclear magnetic resonance, differential scanning calorimetry, thermogravimetric analysis, lipase biodegradation, tensile and cup method testing. All the copolyesters had a weight-averaged molecular weight over 61,000 g/mol or intrinsic viscosity over 1.1 dL/g when the 2,5-furandicarboxylic acid content was in the range from 2 to 10% of terephthalic acid content. Particularly, the tensile strength, yield strength, elongation at break, molecular weight and water vapor barrier of copolyesters were improved to different extents. Obviously, the addition of 2,5-furandicarboxylic acid did not significantly affect the glass transition temperature and thermal stability of polyesters. When the addition amount of 2,5-furandicarboxylic acid was 10%, the water vapor barrier of copolyester reached the highest, which was increased by 89% compared with

Handling Editor: Maude Jimenez.

Address correspondence to E-mail: liyingchun@nuc.edu.cn; zguo10@utk.edu; nanomaterials2000@gmail.com

https://doi.org/10.1007/s10853-022-07269-7

PBAT. On the whole, the copolyesters with the addition of 6% of 2,5-furandicarboxylic acid had the best comprehensive performance, which was conducive to promoting the application of biodegradable agricultural mulching and food packaging film.

GRAPHICAL ABSTRACT

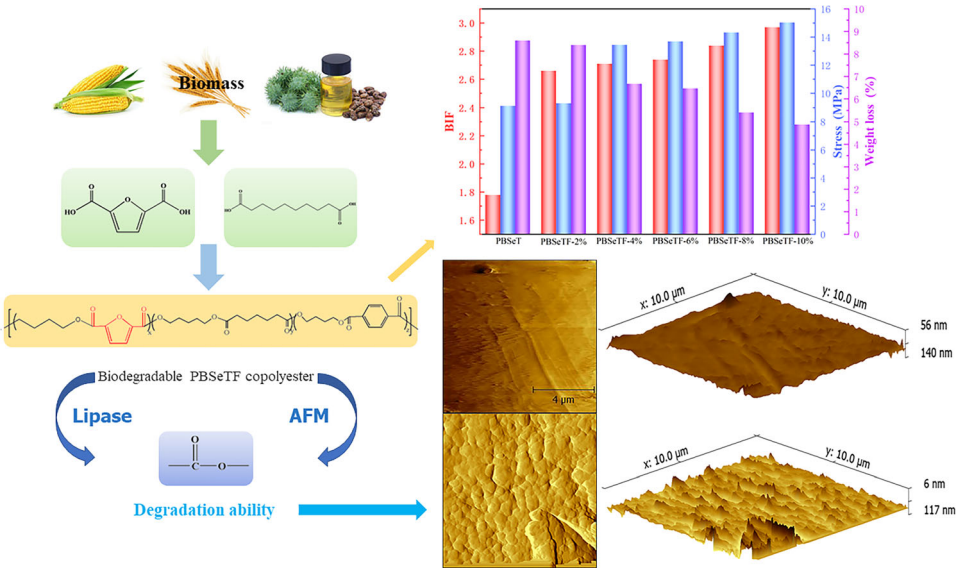

Introduction

With the increasing awareness of environmental protection [1–10] and increasing usage of energy [11–15], bio-based and biodegradable materials have attracted tremendous interest from researchers with their sustainable development and environmental friendly concepts [16–28]. Aliphatic copolyesters stand out from many materials due to their good biodegradability. Poly(butyl succinate) (PBS), poly(lactic acid) (PLA) and poly(butylene adipate-co-terephthalate) (PBAT) [29] have been widely applied in the fields of food packaging, biomedicine, disposable products [30–33]. Although these polymers have gained widespread commercial acceptance, they have been criticized for relying on petrochemicals for their raw materials [34–38]. For example, 1,10-sebacic acid, 1,3-butanediol, 2,5-furandicarboxylic acid and other bio-based monomers have been utilized to synthesize superior bio-based polyesters or copolyesters [39–46].

With the development of the fermentation industry and the massive production of castor oil, sebacic acid (SeA) has become a crucial chemical raw material. SeA is prepared by using castor oil, adipate, butadiene and naphthalene as raw materials via pyrolysis, hydrolysis and decolorization acidification [10, 47–49]. Ricin oleic acid is synthesized from castor oil through catalytic hydrolysis or alkali saponification, and then by alkali cracking with phenol as a diluent. SeA is obtained through the acidification treatment [50, 51]. 2,5-Furandicarboxylic acid (FDCA) is a furan derivative derived from the dehydration of fructose and glucose into 5-carboxymethyl furfural (HMF) and its oxidation [52, 53]. Due to the similar chemical structure with a benzene ring, FDCA is expected to replace terephthalic acid [54, 55]. In recent years, it has been widely used in the synthesis of copolyesters, such as poly(ethylene 2,5-furandicarboxylate) (PEF) [56–60], poly(butylene 2,5-

furandicarboxylate) (PBF) [61], poly(propylene 2,5-furandicarboxylate) (PTF), poly(neopentyglycol 2,5-furandicarboxylic) (PNF) and poly(propylene 2,5-furandicarboxylate) (PPF) [62–65]. However, the properties of bio-based copolyesters are still inadequate compared with traditional petrochemical products.

In recent years, SeA and 2,5-furandicarboxylic acid have rarely been used together as synthetic monomers. For example, Zeng et al. studied the isothermal crystallization performance of poly(butanediol sebacate-butanediol terephthalate) (PBSeT) endow with the content of SeA 5% and 10% [66]. For the mechanical properties, Li et al. investigated the enhancement of puncture resistance of cross-linked poly(butanediol sebacate–butanediol terephthalate) (PBSeT) with different contents of glycerol [67]. Park et al. successfully synthesized PBSeT with a high molecular weight (M_w, 88,700–154,900 g/mol) through adopting DMT instead of TPA. The prepared has excellent 1600% elongation at break of PBSeT64 (sebacic acid/dimethyl terephthalate molar ratio of 6:4) [67]. Valle et al. reported on PBSeT blends through electrospinning of single solutions of PBT and PBSeT mixtures and coelectrospinning of independent PBT and PBSeT solutions. They used a low molecular weight PBSeT with a high ratio of aliphatic sebacate units (i.e., 70 mol% with respect to the total dicarboxylate content) to get new electrospun biodegradable scaffolds [68]. Reports on the use of furanediformic acid as monomer, Hu et al. obtain superior barrier properties by modification of poly (butylene 2,5-furandicarboxylate) with lactic acid [62]. Wang et al. modified poly(ethylene 2,5-furandicarboxylate) with 1,4-cyclohexanedimethylene, which greatly improved its carbon dioxide and oxygen barrier performance [59]. Fully bio-based poly(succinate-co-propylene furandicarboxylate) copolyesters were synthesized from propylene glycol and dimethyl succinic by Hu et al. [63]. The barrier performance of PBAT and PLA has been greatly improved compared with commercial biodegradable materials. To sum up, the effects of different chemical compositions and blends on PBSeT performance have been studied. But there has been no report on how the water vapor barrier properties of PBSeT are relatively scarce.

In the study, a kind of aliphatic copolyester poly(butanediol sebacate–butanediol terephthalate) (PBSeT) was synthesized by partially introducing furan units. The chain structure was characterized by fourier infrared spectroscopy (FTIR), nuclear magnetic resonance hydrogen spectroscopy (^{1}H NMR) and intrinsic viscosity testing, Furthermore, thermodynamic performance and water vapor barrier properties were evaluated by DSC, XRD, TGA, tensile and cup method testing. This kind of copolyester shows the change regulation of water vapor barrier properties with the increase in the content of 2,5-furandicarboxylic acid. The effects of the content of 2,5-furandicarboxylic acid in copolymer composition on the thermodynamic properties and biodegradation of PBSeT were fully discussed.

Experimental

Materials

Sebacic acid (SeA) was kindly provided by Hengshui Jinghua Chemical Industry Co., Ltd. Terephthalic acid (TPA), 1,4-butanediol (BDO), 2,5-furandicarboxylic acid [Aladdin Reagent Co., Ltd. (Shanghai, China)], tetrabutyl titanate (TBOT, Wuxi Yatai United Chemical Co., LTD.), chloroform (Tianjin Shentai Chemical Reagent Co., LTD.), phenol (Guangzhou Chemical Reagent Factory), tetrachloroethane (Shanghai Chemical Industry Park) and methanol (Tianjin Hengxing Chemical Reagent Manufacturing Co. Ltd.) were all used as received.

Synthesis of PBSeT and PBSeTF-X copolymers

In a 5-L reaction kettle, poly(butanediol sebacate-butanediol terephthalate) was synthesized via two-step esterification and polycondensation. The first esterification stage was carried out during 160–180 °C under atmospheric pressure, and then, BDO (3.5 mol), furanediformic acid and sebacic acid (3.5 mol) were added into the reaction kettle under agitation for 1–2 h. The temperature was raised to 220 °C for the second stage esterification reaction, TBOT (0.3% acid content), terephthalic acid (3.5 mol) and BDO (1.5 mol) were added at the same time, and the reaction lasted for 3–4 h. At the end of the esterification stage, the pressure was gradually reduced to 220–700 Pa when the discharge was close to the theoretical water value generated by the reaction, and TBOT was introduced into the reaction kettle to start the polycondensation stage. In the polycondensation

stage, 4–5 h were carried out during 240–250 °C, and the reaction ends when the torque value of the control box of the reaction kettle does not change. The polyesters synthesized in the reactor were removed at room temperature and purified to obtain white solid products. The product was dissolved in trichloromethane and then precipitated with excessive cold methanol to obtain white floccule products, which were dried at 40 °C for 24 h.

The polyesters synthesized using 2,5-furandicarboxylic acid amounts of 0 mol, 0.07 mol, 0.14 mol, 0.21 mol, 0.28 mol and 0.35 mol were symbolized as PBSeT, PBSeTF-2%, PBSeTF-4%, PBSeTF-6%, PBSeTF-8% and PBSeT-10%, respectively.

Characterizations

ATR-FTIR spectra of the copolyesters were recorded with a Nicolet iS10 spectroscopy (Thermo Fisher Scientific, USA) equipped with a ZnSe crystal ATR accessory. The scan range was from 500 to 4000 cm^{-1}, and each sample was scanned for 32 times. Disk specimens were prepared using a precision thermostat table and a hot-press molding at 180 °C.

^1H NMR spectra were recorded with a Bruker AVANCE-3 HD spectroscopy (600 M). Deuterated chloroform was used as solvent and tetramethylsilane as the internal reference. After the NMR tube was cleaned by ultrasonic vibration, deuterium chloroform was used as solvent to dissolve the sample, and tetramethylsilane was used as internal reference for testing.

Polydispersity (PDI), the number-averaged molecular weight (Mn) and weight-averaged molecular weight (Mw) were determined at 35 °C with a gel permeation chromatography (GPC, Waters Co., USA) equipped with a differential refractive index detector. Tetrahydrofuran was used as eluent at a flow rate of 1.0 mL/min.

The intrinsic viscosity [η] of all samples dissolved in the phenol/1,1,2,2-tetrachloroethane mixture was measured using a Ubbelohde viscometer at 25 °C. The inner diameter of the capillary tube of the Ubbelohde viscometer is 0.88 mm. The mass ratio of phenol to 1,1,2,2-tetrachloroethane is 1:1.

Thermal transition behaviors were recorded with differential scanning calorimetry (DSC-1, METTLER TOLEDO) under a nitrogen flow condition. Approximately 7–8 mg of the sample was tested under a standard heat–cool–heat cycle from − 60 to 200 °C, and both heating and cooling rates were 10 °C/min. The temperature was kept at 200 °C for 5 min before cooling, and the thermal history was eliminated.

X-ray diffraction (XRD) pattern was recorded using a RIGAKU X-ray diffraction system (D/max-Rb) with Cu radiation (1.54 Å), working at 40 kV and 100 mA. The samples were scanned from $2\theta = 5°$ to $2\theta = 50°$with a step size of 0.01°and an acquisition time of 30 s per step.

Thermogravimetric analysis (TGA) measurements were taken under an argon atmosphere by a thermal analyzer (TGA, TG290, NETZSCH) from 10 to 600 °C at a 10 °C/min heating rate.

Tensile properties were measured with a CMT6104 universal testing machine at a tensile speed of 50 mm/min. Dumbbell-shaped tensile specimens were prepared by injection molding. All the specimens were kept in a standard atmosphere of 25 °C for at least 24 h before testing. At least five specimens were tested for each sample, and all the reported properties were presented average values of all the trials.

According to GB 1037-1988, the cup method is used to measure water vapor transmittance (WVTR) of sheet metal. Dry $CaCl_2$ is added to a hygroscopic cup; then, the sample film is covered and sealed with sealing wax. The sealing wax formula is a mixture of 85% paraffin wax and 15% beeswax. In an incubator with a constant temperature (38 °C) and humidity (90 RH%), place the permeable cup. Record the total weight of the test cup over time. Due to the strong hygroscopicity of dried $CaCl_2$, the relative humidity (RH) inside the cup is close to zero, so the added weight is close to the weight of the water passing through the sample. Water vapor permeability PWV was calculated with Eq. (1), where d is the thickness of the film, WVT is water vapor transmission, P_0 is the saturated water vapor pressure (6630 Pa at 38 °C), and RH_1 and RH_2 are the relative humidities on both sides of the film.

$$P_{WV} = \frac{WVT \times d}{p^0(RH_1 - RH_2)} \quad (1)$$

Copolyester in the form of films 1 × 1 cm in size and 0.3 mm thickness was prepared by a hot-press molding at 180 °C with a precision thermostat. It was placed in a vial containing 0.8 mg/mL phosphate buffer (pH 7.4) of lipase at 37 °C. The media were replaced every 7 days. The films were removed from

the vial every 7 days, washed with distilled water, dried under vacuum, and weighted until they reached a constant weight. The degree of biodegradation was estimated from the weight loss.

The change in the surface morphology upon degradation was evaluated by scanning atomic force microscope (AFM, Cypher ES from AsylumResearch, USA). The sample is a degraded copolyester sample with a size of 1 × 1 cm in size and 0.3 mm thickness.

Results and discussion

Synthesis and structure characterization

Poly(butanediol sebacate-butanediol terephthalate)s with 2,5-furandicarboxylic acid were synthesized via a two-step esterification and polycondensation process, just as shown in Scheme 1. TBOT was adopted as a catalyst for every steps. In terms of monomers used in this study, SeA and 2,5-furandicarboxylic acid are bio-based, while terephthalic acid and 1,4-butanediol are petroleum-based monomers.

The reaction conditions and test results of copolyesters are summarized in Table 1. Because the prepolymerization stage is designed to ensure the full synthesis of 2,5-furandicarboxylic acid, the esterification stage of PBSeTF copolyester is divided into two parts. But it is worth noting that the aggregate time decreases. The intrinsic viscosity [η] of the copolyester measured by phenol/tetrachloroethane mixture solution (1/1 w/w) was more than 1.10 dL/g except for PBSeTF-2%. The average molecular weight of all copolyesters was more than 61,000 g/mol. Compared with PBSeT, the average molecular weight of PBSeTF with 2,5-furandicarboxylic acid was improved. The relative molecular weight and characteristic viscosity of copolymers are similar, indicating that high molecular weight polymers have higher relative molecular weight [69, 70].

The chemical structure of the copolymers was determined by FTIR and ^{1}H NMR. Figure 1 shows the FTIR spectra of PBSeT and PBSeTF-X copolymers. The stretching vibration of C–O–C and the contraction vibration of C–O appear at 1104, 1216 and 1713 cm^{-1}. The strong signal at 2851 and 2928 cm^{-1} were a distinct aliphatic band, all two of which proved the existence of ester group. In addition, C–H stretching vibration absorption peaks of adjacent benzene ring at 726 cm^{-1} and two C–O signals belonging to aromatic group were observed at 1269 and 1540 cm^{-1}. It is worth noting that the weak side of the hydroxyl absorption peak is at 3400 cm^{-1}, indicating that the copolymer has a high molecular weight. Increasing the amount of 2,5-furandicarboxylic, the spectra of PBSETF-X showed the C–H bending vibration of the furan ring at 757 and 956 cm^{-1} the C=C absorption peak at 1576 cm^{-1}. The intensity of these signals increased with m_f. It was proved that 2,5-furandicarboxylic acid was

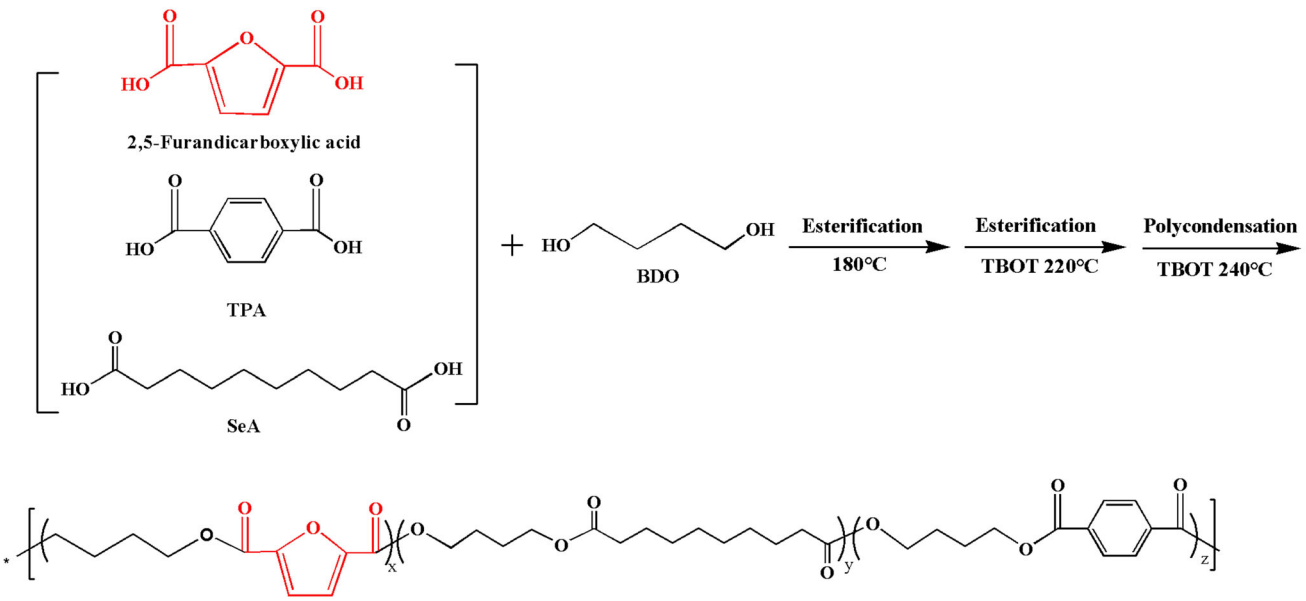

Scheme 1 Schematic diagram of synthesis of PBSeTF-X.

Table 1 Synthetic conditions and results of the eight poly(butylene sebacate-co-terephthalate)s

Sample	Φ_{FDCA}[a] (mol)	T_{es}/t_{es}[b]	T_{mp}/t_{mp}[c]	$[\eta]$[d] (dL/g)	GPC		
					Mn (g/mol)	M_w (g/mol)	PDI
PBSeT	0	220/3.5	240/6	1.02	61,202	74,167	1.21
PBSeTF-2%	0.07	180/1.5 + 220/2.5	240/5.5	1.05	61,072	75,943	1.24
PBSeTF-4%	0.14	180/1.5 + 220/2.5	240/5	1.15	66,748	74,533	1.12
PBSeTF 6%	0.21	180/1.5 + 220/2.5	240/4.5	1.24	72,874	77,247	1.06
PBSeTF-8%	0.28	180/1.5 + 220/2.5	240/5	1.39	79,346	82,511	1.04
PBSeTF-10%	0.35	180/1.5 + 220/2.5	240/4.5	1.20	71,594	79,630	1.11

(1) Esterification: TBT, 0.6 mol% based on diacid was used as catalyst; diol/diacid molar ratio 1.2. (2) Polycondensation: additional 0.3 mol% TBT was added

[a]The moles of 2,5-furandicarboxylic acid

[b]Esterification temperature and time

[c]Melt polycondensation temperature and time

[d]Intrinsic viscosity was measured at 25 °C using a mixture of phenol-tetrachloroethane with a mass ratio of 1:1 as solvent

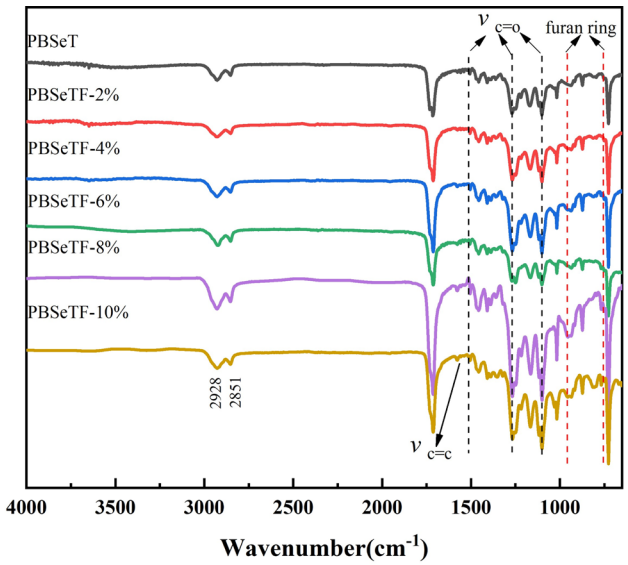

Figure 1 ATR-FTIR spectra of the PBSeT (CS) and PBSeTF-X.

successfully polymerized on the molecular segment of the original PBSeT copolymer. PBSeT and PBSETF-X in ATR-FTIR were combined to confirm the successful synthesis of a novel copolymer with furan segments.

^{1}H NMR spectra of the six poly(butanediol sebacate-butanediol terephthalate)s are shown in Fig. 2a. The^{1}H NMR spectra of PBSeTF-10% are presented in Fig. 2b. The chemical shift of chloroform was located at 7.25 ppm. The chemical structure of the furan ring is very similar to that of the benzene ring, and the chemical shift of the hydrogen atoms of the methylene near the furan ring is similar to that near the benzene ring. Take the benzene ring as an example to explain possible triads for PBSeTF in Fig. 2c. For the same structural parts of PBSeT and PBSeTF-X, in the BDO of three possible triads, the two CH_2 (a1, a2, a3, a4) near the oxygen atom split into four different signals at δ = 4.08, 4.14, 4.38 and 4.43 ppm, respectively. Similarly, in BDO, the two CH_2 (b1, b2, b3, b4) far from the oxygen atom also split into four distinct signals δ = 1.97, 1.86, 1.80 and 1.69 ppm. In addition, the chemical shift of hydrogen (d) on benzene rings in TBT and TBS units is δ = 8.09 ppm. In PBSeT and PBSETF-X chain segments, the chemical shifts of hydrogen atoms (c) near the ester group and hydrogen atoms (f) far from the ester group in SeA monomer part are δ = 1.30 and 2.28 ppm, respectively. For PBSeTF-X chemical structure, the chemical shift of hydrogen of the furan ring is 7.22 ppm, and the signal intensity increases with the increasing content of 2,5-furandicarboxylic acid. Combined with the results of ATR-FTIR and ^{1}H NMR, PBSeT and PBSETF-X copolyesters with the expected chemical structure were successfully synthesized.

Thermal transition

The multi-section scanning DSC curves of PBSeT and PBSeTF are shown in Fig. 3, and the thermal transformation data are listed in Table 2. PBSeT and PBSeTF both crystallized and melted under a typical

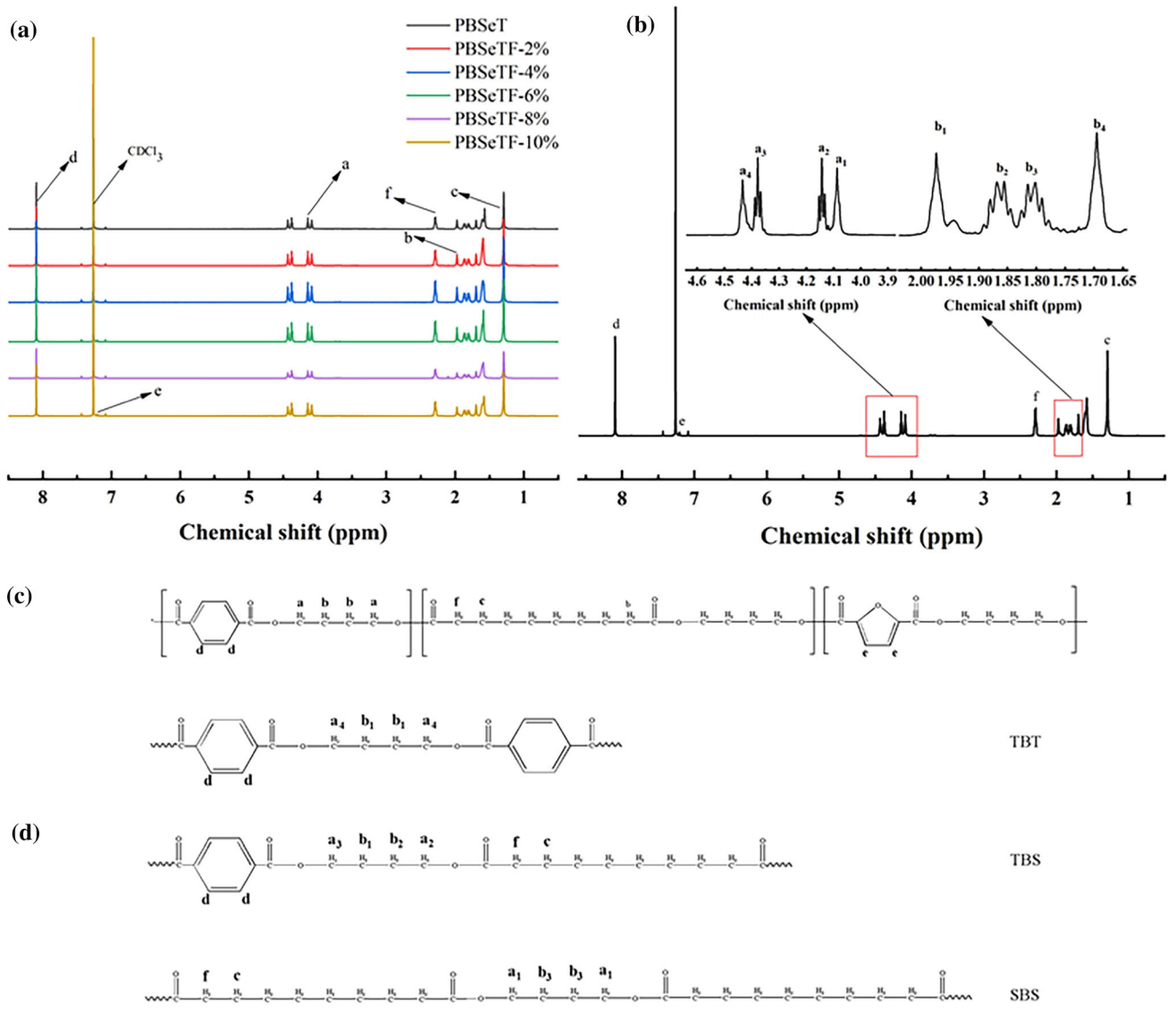

Figure 2 **a** ^{1}H NMR spectra of the PBSeT and PBSeTF-X; **b** chemical structure and^{1}H NMR spectra of PBSeTF-10%; **c** three possible triads for PBSeT; **d** chemical structural formulas for different chemical displacements are indicated.

cooling and heating rate of 10 °C/min, and all samples had a single T_g. This shows that the different components of the chain segment in polyester have good compatibility. In the cooling scan, with the increase in the content of furaric acid, the exothermic peak T_c generated by crystallization of PBSeT gradually moved to low temperature. However, during the cooling process, ΔHC decreased first and then increased. The main reason is that the original structure of the chain segment is broken when the content of furan ring introduced is small, and the structure similar to benzene ring can be restored when the amount of furan ring introduced is not broken and increased. Additionally, due to the strong rigidity and poor geometric symmetry of the furan unit, the crystallization capacity of the introduced furan polyester is less than that of the terephthalate polyester [71]. The crystallinity of copolyesters decreased first and then increased, and the crystallinity X_C ranged from 8.66 to 10.83%. The crystallization degree of PBSeTF copolyester reached highest when the incorporation of 2,5-furandicarboxylic acid was 8%.

The copolymers of PBSeT and PBSeTF showed a melting peak and glass transition during the second heating. The glass transition temperature (T_g) varies

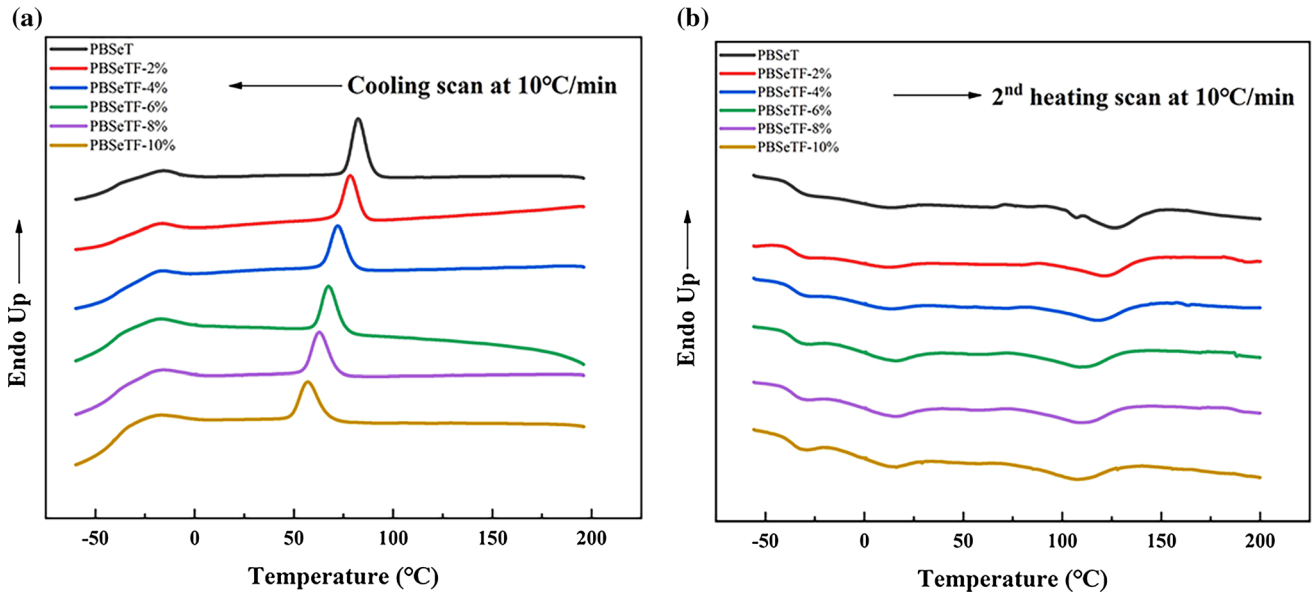

Figure 3 DSC thermograms of PBSeT (CS) and PBSeT (GL-X): **a** cooling scan at − 10 °C/min, **b** 2nd heating scan at 10 °C/min.

Table 2 Thermal transition properties of PBSeT (CS) and PBSeT (GL-X)

Sample	Cooling scan		Second heating scan		X_C%
	T_c	ΔH_C	T_g	T_m	
PBSeT	82.54	19.10	− 43.85	126.56	10.83
PBSeTF-2%	78.43	15.26	− 41.32	121.95	8.66
PBSeTF-4%	71.99	16.73	− 43.65	118.73	9.48
PBSeTF-6%	67.49	17.07	− 43.35	111.57	9.67
PBSeTF-8%	62.79	17.77	− 43.30	109.07	10.23
PBSeTF-10%	57.14	17.50	− 43.53	108.53	10.01

slightly from 41.32 to 43.85 °C, while the melting temperature (T_m) varies greatly from 108.53 to 126.56 °C. The types of melting peaks of PBSeT and PBSeTF hardly change and move to the low-temperature region.

In order to further understand the crystal structures of PBSeT and PBSeTF, X-ray diffraction experiments were carried out on the samples. The XRD patterns are shown in Fig. 4. The XRD pattern clearly shows that PBSeT and PBSeTF have similar crystal structures and both belong to weak crystalline polymers. As shown in Fig. 4, PBSeT and PBSeTF crystals have the same diffraction peaks at 17.4° (010), 20.5° (101), 23.1° (100) and 24.8° (111). The diffraction peak position of the two crystals is roughly the same as that of PBT, indicating that the crystalline part of copolyester is mainly contributed by BT unit [72]. The

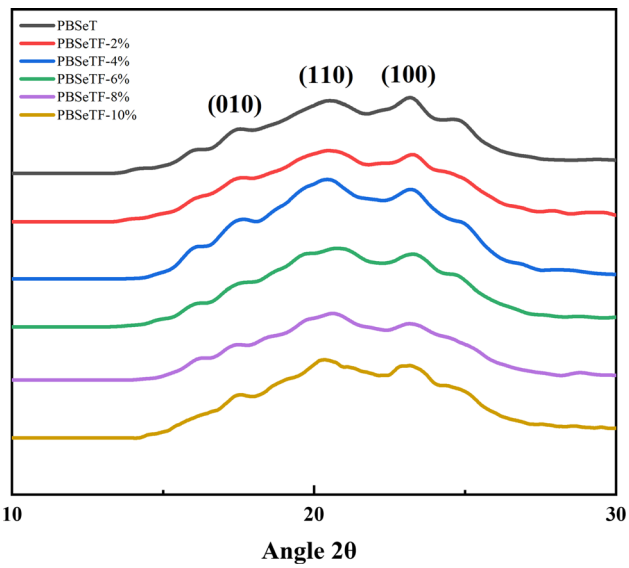

Figure 4 XRD patterns of the indicated PBSeT and PBSeTF-X.

addition of 2,5-furandicarboxylic acid do not affect the crystal shape of PBSeT, but retained the original crystal shape.

Thermal stability

In order to study the thermal stability of copolyesters, thermogravimetric analysis was carried out on the samples. Thermogravimetric and differential thermogravimetric curves in nitrogen atmosphere are shown in Fig. 5. The decomposition temperature at 5% weight loss, maximum decomposition rate

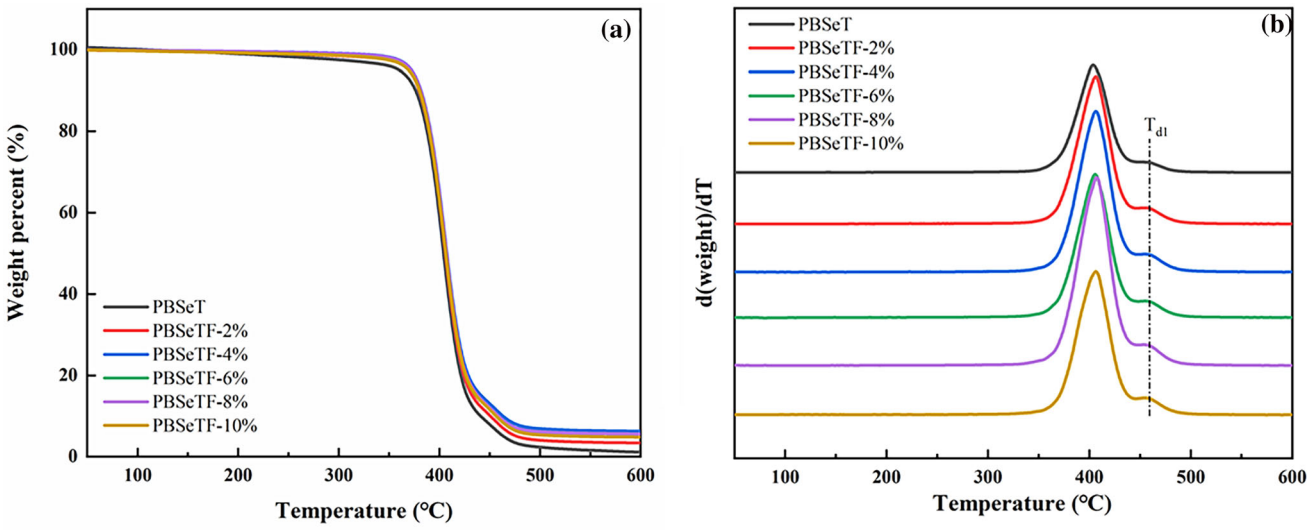

Figure 5 **a** Thermogravimetric and **b** differential thermogravimetric curves of the indicated PBSeT and PBSeTF (10 °C/min, Ar).

Table 3 Characteristic decomposition temperatures of PBSeT and PBSeTF copolyesters

Sample	$T_{d,5}$ (°C)	$T_{d,max}$ (°C)	T_{d1} (°C)	Residue at 600 °C (%)
PBSeT	352.0	403.3	459.3	2.56
PBSeTF-2%	369.3	406.1	460.1	3.36
PBSeTF-4%	372.0	406.6	459.3	6.30
PBSeTF-6%	372.0	406.0	458.6	5.97
PBSeTF-8%	372.7	407.3	459.3	5.62
PBSeTF-10%	369.3	406.7	460.0	4.83

temperature and residual weight at 600 °C are listed in Table 3. When the temperature was lower than 300 °C, all samples were in a stable state without decomposition. It could be seen that the copolyesters showed no obvious instability front and back the incorporation of 2,5-furandicarboxylic acid. The main degradation temperature of all samples was between 350 and 420 °C. The maximum decomposition rate ($T_{d,max}$) of the polymer was in the small temperature range of 403 to 407 °C. Obviously, compared with PBSeT, PBSeTF copolyesters showed higher $T_{d,5}$, $T_{d,max}$ and char residues. These characteristic temperatures increase with increasing the content of 2,5-furandicarboxylic acid. For example, $T_{d,5}$ and $T_{d,max}$ of PBSeTF-8% are 20 °C and 5 °C higher than PBSeT, respectively. Relatively high $T_{d,5}$ of samples suggested relatively high molecular weight and relatively narrow molecular weight distribution, in accordance with the results of GPC [65]. In the tested temperature range, the residual char content of PBSeTF copolyethylene was also higher than that of PBSeT, mainly because the introduction of aromatic furan rings increased the content of residual char content. The results show that PBSeTF copolyester has better thermal stability than PBSeT. PBSeTF can be safely processed without thermal degradation at 50–60 °C above its corresponding T_m.

Mechanical properties

In this part, the mechanical properties of PBSeT and PBSeTF are evaluated by tensile test. The stress–strain curves of PBSeT and PBSeTF are shown in Fig. 6. The tensile properties of samples are summarized in Table 4, including Young's modulus (E), tensile strength (δ_b), yield strength (δ_y) and elongation at break (ε_b).

The PBSeT copolyester exhibits obvious tensile behavior of a semicrystalline flexible polymer. PBSeT copolyester exhibits optional semicrystalline flexible polymer tensile behavior, with the apparent yield point before fracture with Young's modulus of 7.81 MPa of 9.13 MPa and of 1425.11%. At the same time, the yield strength is only 4.91 MPa, indicating that its stability is poor when it can be restored to its

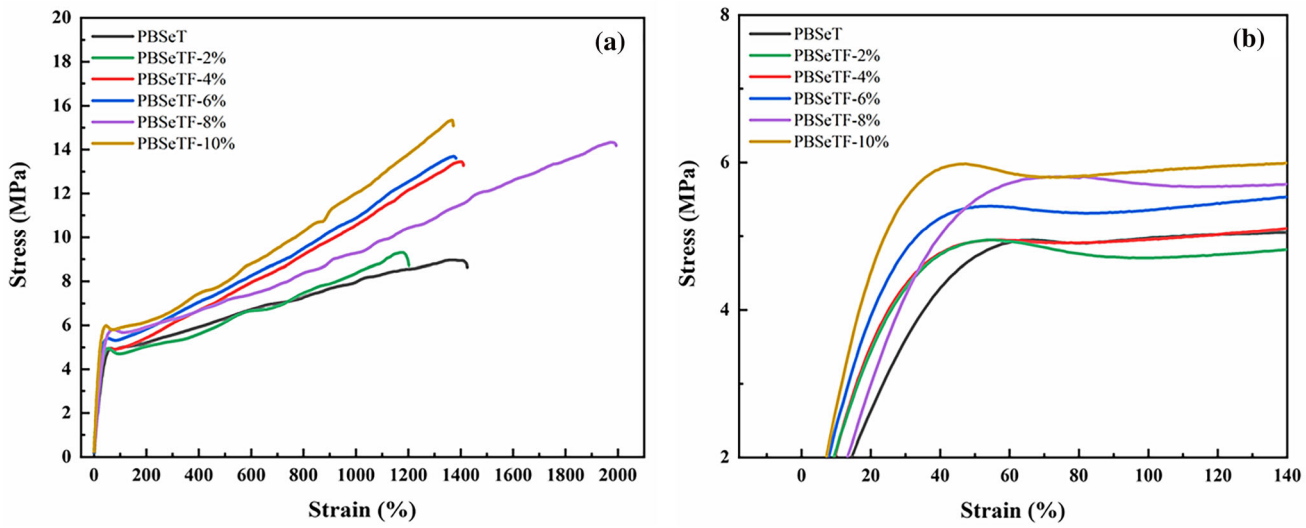

Figure 6 **a** Stress–strain curves of PBSeT and PBSeTF. **b** Enlarged view of yield point.

Table 4 Mechanical properties of PBSeT and PBSeTF-X

Sample	E (MPa)	δ_b (MPa)	δ_y (MPa)	ε_b (%)
PBSeT	7.81 ± 0.21	9.13 ± 0.53	4.91 ± 0.22	1425.11 ± 44.01
PBSeTF-2%	8.89 ± 0.46	9.31 ± 0.43	4.94 ± 0.23	1203.55 ± 52.23
PBSeTF-4%	9.40 ± 0.55	13.45 ± 0.42	4.95 ± 0.36	1410.91 ± 43.56
PBSeTF-6%	10.21 ± 0.23	13.69 ± 0.65	5.41 ± 0.21	1381.99 ± 70.24
PBSeTF-8%	8.50 ± 0.23	14.33 ± 0.58	5.81 ± 0.43	1993.77 ± 67.33
PBSeTF-10%	12.67 ± 0.37	15.04 ± 0.41	5.92 ± 0.34	1371.87 ± 32.31

original state after elastic deformation by external force. With the introduction of furan ring, the tensile strength of PBSeTF increased from 9.31 to 15.3 MPa. The main reason may be that the furan element was tough and rectangular compared with the benzene ring element itself, which led to the continuous increase in the tensile strength. Figure 6b shows that PBSeTF has better yield strength compared with PBSeT, which increases from 4.91 to 5.92 MPa, mainly because the furan ring has better rigidity compared with benzene ring. With the increase in the proportion of furan ring, the rigidity of the whole polymer molecular chain segment increases, and thus, it has better yield strength. With the increase in the molecular chain segment rigidity, the elongation at break of PBSeTF polyester except PBSeTF-8% decreased to different degrees, ranging from 1203.55 to 1410.91%. It is interesting that the elongation at break of PBSeTF-8% sample is 1993.77%, and the elongation at break is also significantly increased when the tensile strength and yield strength are improved, which may be mainly caused by the highest molecular weight in all the samples, and the decrease in its crystallinity may be one of the reasons.

To sum up, the mechanical properties of PBSeT and PBSeTF depend on their composition, crystallinity, molecular weight and many other factors. Compared to PBSeT, PBSeTF has excellent mechanical properties.

Water vapor barrier properties

PBAT and PLA are two of the most widely used biodegradable thin-film materials in the current market. The water vapor permeability coefficient (p_{wv}) of PBSeT, PBSeTF, PBAT and PLA was compared at 38 °C and 90% RH. The experimental results are shown in Table 5. Using PLA sample as a standard, the barrier improvement factor (BIF) is defined as P_{PLA}/P_{PBSeTF}. The improvement in vapor barrier was reflected by the BIF. Table 5 shows that with the introduction of furandiformic acid, the water vapor barrier performance of PBSeT copolepster increases linearly. Compared with PLA, PBAT and PBSeT, the vapor barrier of PBSETF-10% increases by 66.4%,

Table 5 Water vapor barrier properties of PBSeT (CS) and PBSeT (GL-X)

Sample[a]	P_{wv}[b]	BIF[c]
PLA	1.1×10^{-13}	1
PBAT	3.52×10^{-13}	0.31
PBSeT	6.19×10^{-14}	1.78
PBSeTF-2%	4.13×10^{-14}	2.66
PBSeTF-4%	4.06×10^{-14}	2.71
PBSeTF-6%	4.01×10^{-14}	2.74
PBSeTF-8%	3.87×10^{-14}	2.84
PBSeTF-10%	3.70×10^{-14}	2.97

[a]Water vapor permeation: dish method, 38 °C, RH = 90%

[b]Water vapor permeability coefficient with unit of g cm cm^{-2} s^{-1} Pa^{-1})

[c]Barrier improvement factor (BIF) is defined as P_{PLA}/P_{PBSeTF}

[d]Water vapor transmission rate, at 38 °C, 90% relative humidity

89.5% and 40.2%, respectively. The main reason for the improvement of water vapor barrier is that the furan ring has better rigidity than the benzene ring, and the water vapor barrier increases with the increase in the number of furan rings. The higher molecular weight may also play a positive role in water vapor barrier. The higher molecular weight may also play a positive role in the water vapor barrier. Polymers with a higher molecular weight have more long chains mathematically and statistically than polymers with lower molecular weight, and longer polymer chains are bound to provide better barrier properties.

Biodegradation of PBSeF and PBSeTF

The degradation performance of PBSeT and PBSeTF in lipase culture was investigated. The degradation capacity of the polymer was characterized by the proportion of mass loss at 7, 14, 21 and 28 days. Figure 7 shows the experimental results of significant weight loss of the polymer over time. The results were as expected; with the introduction of the furan ring, the polymer had a smaller weight loss during enzymatic degradation. The decrease in the weight loss may be the increase in the steric hindrance in molecular chain segment due to the introduction of the furan ring, which leads to the degradation behavior onto the ester bonds by the degradation enzymes was sterically hindered [50].

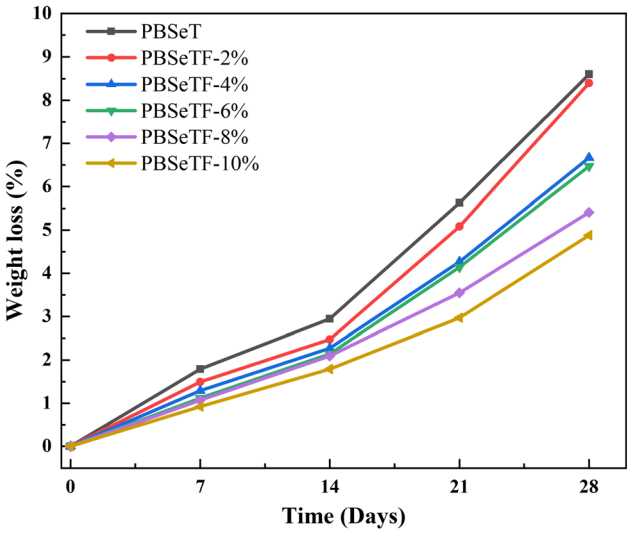

Figure 7 Weight loss curves of PBSeT and PBSeTF during enzymatic degradation.

In order to explore the changes of surface morphology after degradation, AFM scanning was carried out front and back polyester degradation. Before degradation, the sample surface was relatively smooth, as shown in Fig. 8 (0 day). However, the surface of the degraded samples is rough, concave and undulating, and presents different forms according to the content of 2,5-furandicarboxylic acid. The display is circumstance through roughness curves and 3D images. The results of AFM were consistent with those of enzyme degradation experiments, and the degradation ability of copolyesters was weakened by adding 2,5-furandicarboxylic acid.

Conclusions

Using sebacic acid, terephthalic acid and 1,4-butanediol as raw materials, and 0.07–0.35 mol of 2,5-furandicarboxylic acid as the fourth monomer, polybutylene sebacate-butanediol terephthalate was synthesized via two-step esterification and polycondensation. Compared with PBSeT, with the addition of furan dicarboxylic acid, the tensile strength, yield strength and water vapor barrier of PBSeTF are obviously enhanced. At the same time, the excellent thermal stability at 300 °C ensures the processing performance of copolyesters in industrial production. Nonetheless, due to the addition of furan dicarboxylic acid, the crystallinity of PBSeTF copolyester first decreased and then increased, while the T_m and

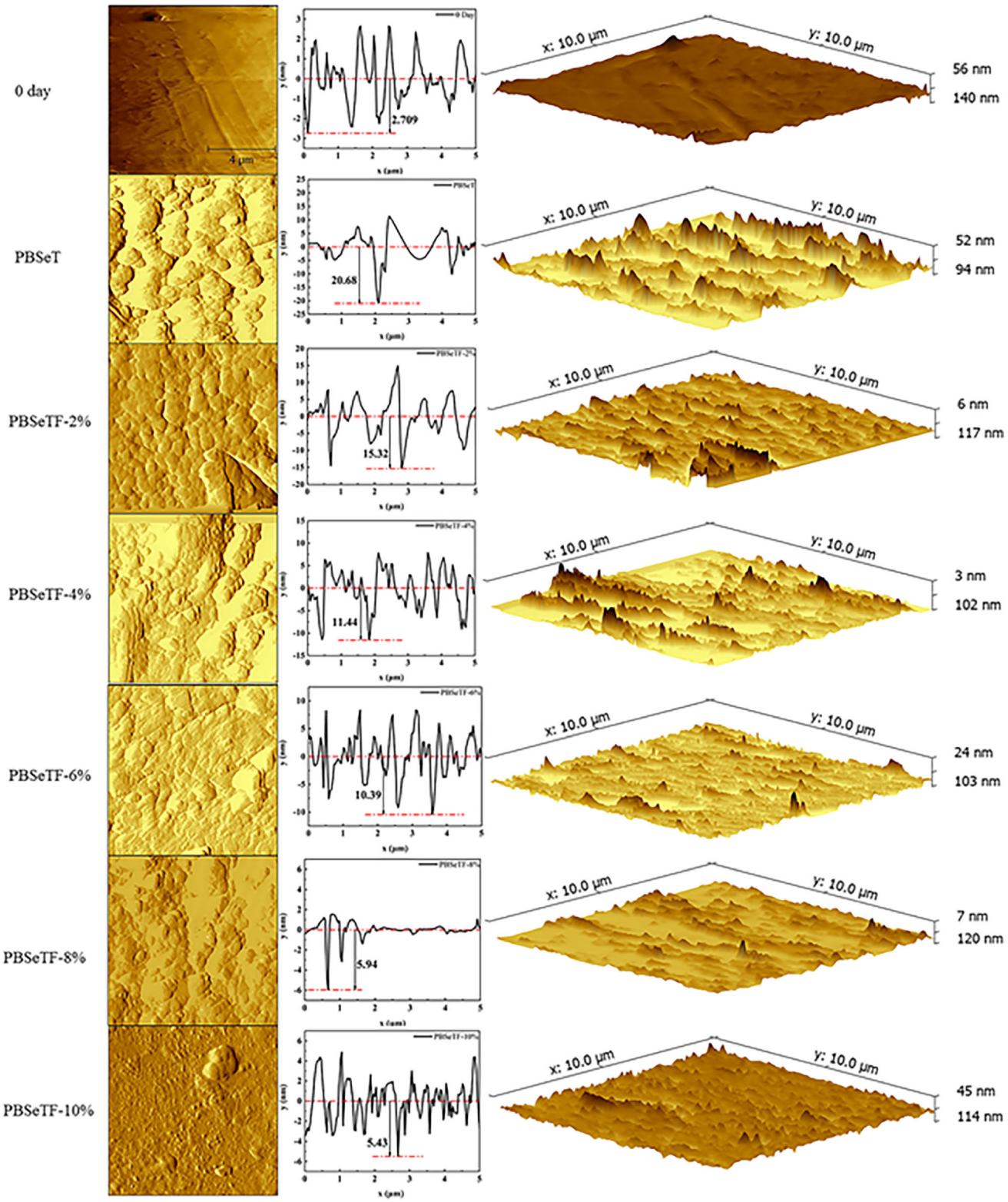

Figure 8 AFM images of PBSeT and PBSeTF surfaces before and after enzyme degradation (28 days), roughness curve and 3D images.

degradation properties decreased. Fortunately, the water vapor barrier performance of PBSeTF copolyester has been significantly improved, which is crucial to improving the degradability and performance of composite agricultural films and food packaging films. Therefore, aliphatic–aromatic

copolyesters with furan as an additive monomer can become a new kind of membrane material. Future research will focus on improving the crystallinity, crystallization capacity and mechanical properties of copolyesters.

Acknowledgements

The authors acknowledge the financial support of Taif University Researchers Supporting Project Number (TURSP-2020/27), Taif University, Taif, Saudi Arabia.

Declarations

Conflict of interest The authors declare that they have no known competing financial interests or personal relationships that could have appeared to influence the work reported in this paper.

References

[1] Ahmadi SAR, Kalaee MR, Moradi O, Nosratinia F, Abdouss M (2021) Core–shell activated carbon-ZIF-8 nanomaterials for the removal of tetracycline from polluted aqueous solution. Adv Compos Hybrid Mater 4:1384–1397. https://doi.org/10.1007/s42114-021-00357-3

[2] Chai J, Hu Q, Qiu B (2021) Conductive polyaniline improves Cr(VI) bio-reduction by anaerobic granular sludge. Adv Compos Hybrid Mater 4:1137–1145. https://doi.org/10.1007/s42114-021-00342-w

[3] Deng Z, Deng Q, Wang L et al (2021) Modifying coconut shell activated carbon for improved purification of benzene from volatile organic waste gas. Adv Compos Hybrid Mater 4:751–760. https://doi.org/10.1007/s42114-021-00273-6

[4] Jain B, Hashmi A, Sanwaria S, Singh AK, Susan MABH, Singh A (2020) Zinc oxide nanoparticle incorporated on graphene oxide: an efficient and stable photocatalyst for water treatment through the Fenton process. Adv Compos Hybrid Mater 3:231–242. https://doi.org/10.1007/s42114-020-00153-5

[5] Liang J, Li X, Zuo J, Lin J, Liu Z (2021) Hybrid 0D/2D heterostructures: in-situ growth of 0D g-C3N4 on 2D BiOI for efficient photocatalyst. Adv Compos Hybrid Mater 4:1122–1136. https://doi.org/10.1007/s42114-021-00341-x

[6] Shao Y, Bai H, Wang H, Fei G, Li L, Zhu Y (2022) Magnetically sensitive and high template affinity surface imprinted polymer prepared using porous TiO2-coated magnetite-silica nanoparticles for efficient removal of tetrabromobisphenol A from polluted water. Adv Compos Hybrid Mater. 5:130–143. https://doi.org/10.1007/s42114-021-00361-7

[7] Si Y, Li J, Cui B et al (2022) Janus phenol–formaldehyde resin and periodic mesoporous organic silica nanoadsorbent for the removal of heavy metal ions and organic dyes from polluted water. Adv Compos Hybrid Mater in press: https://doi.org/10.1007/s42114-42022-00446-x.10.1007/s42114-022-00446-x

[8] Wang Y, Xie W, Liu H, Gu H (2020) Hyperelastic magnetic reduced graphene oxide three-dimensional framework with superb oil and organic solvent adsorption capability. Adv Compos Hybrid Mater 3:473–484. https://doi.org/10.1007/s42114-020-00191-z

[9] Yin C, Wang C, Hu Q (2021) Selective removal of As(V) from wastewater with high efficiency by glycine-modified Fe/Zn-layered double hydroxides. Adv Compos Hybrid Mater 4:360–370. https://doi.org/10.1007/s42114-021-00214-3

[10] Zhao Y, Liu F, Zhu K, Maganti S, Zhao Z, Bai P (2022) Three-dimensional printing of the copper sulfate hybrid composites for supercapacitor electrodes with ultra-high areal and volumetric capacitances. Adv Compos Hybrid Mater. https://doi.org/10.1007/s42114-022-00430-5

[11] Dong X, Zhao X, Chen Y, Wang C (2021) Investigations about the influence of different carbon matrixes on the electrochemical performance of $Na_3V_2(PO_4)_3$ cathode material for sodium ion batteries. Adv Compos Hybrid Mater 4:1070–1081. https://doi.org/10.1007/s42114-021-00319-9

[12] Huang J, Chen Q, Chen S et al (2021) Al3+-doped $FeNb_{11}O_{29}$ anode materials with enhanced lithium-storage performance. Adv Compos Hybrid Mater 4:733–742. https://doi.org/10.1007/s42114-021-00291-4

[13] Liu L, Guo Z, Yang J, Wang S, He Z, Wang C (2021) High ion selectivity Aquivion-based hybrid membranes for all vanadium redox flow battery. Adv Compos Hybrid Mater 4:451–458. https://doi.org/10.1007/s42114-021-00261-w

[14] Long Z, Yuan L, Shi C, Wu C, Qiao H, Wang K (2021) Porous Fe_2O_3 nanorod-decorated hollow carbon nanofibers for high-rate lithium storage. Adv Compos Hybrid Mater. https://doi.org/10.1007/s42114-021-00397-9

[15] Xie Y, Yang Y, Liu Y et al (2021) Paraffin/polyethylene/graphite composite phase change materials with enhanced thermal conductivity and leakage-proof. Adv Compos Hybrid Mater 4:543–551. https://doi.org/10.1007/s42114-021-00249-6

[16] Atta OM, Manan S, Ul-Islam M, Ahmed AAQ, Ullah MW, Yang G (2022) Development and characterization of plant oil-incorporated carboxymethyl cellulose/bacterial cellulose/glycerol-based antimicrobial edible films for food packaging

applications. Adv Compos Hybrid Mater. https://doi.org/10.1007/s42114-021-00408-9

[17] Fatima A, Yasir S, Ul-Islam M et al (2021) Ex situ development and characterization of green antibacterial bacterial cellulose-based composites for potential biomedical applications. Adv Compos Hybrid Mater. https://doi.org/10.1007/s42114-021-00369-z

[18] Geyer R, Jambeck JR, Law KL (2017) Production, use, and fate of all plastics ever made. Sci Adv. https://doi.org/10.1126/sciadv.1700782

[19] Huang JH, Cheng XQ, Wu YD et al (2021) Critical operation factors and proposed testing protocol of nanofiltration membranes for developing advanced membrane materials. Adv Compos Hybrid Mater 4:1092–1101. https://doi.org/10.1007/s42114-021-00334-w

[20] Jing X, Li Y, Zhu J et al (2022) Improving thermal conductivity of polyethylene/polypropylene by styrene-ethylene-propylene-styrene wrapping hexagonal boron nitride at the phase interface. Adv Compos Hybrid Mater. https://doi.org/10.1007/s42114-022-00438-x

[21] Kuang T, Ju J, Liu T et al (2022) A facile structural manipulation strategy to prepare ultra-strong, super-tough, and thermally stable polylactide/nucleating agent composites. Adv Compos Hybrid Mater. https://doi.org/10.1007/s42114-021-00390-2

[22] LaChance AM, Hou Z, Farooqui MM et al (2022) Polyolefin films with outstanding barrier properties based on one-step coassembled nanocoatings. Adv Compos Hybrid Mater. https://doi.org/10.1007/s42114-022-00421-6

[23] Luo W, Wei Y, Zhuang Z et al (2022) Fabrication of Ti3C2Tx MXene/polyaniline composite films with adjustable thickness for high-performance flexible all-solid-state symmetric supercapacitors. Electrochim Acta 406:139871. https://doi.org/10.1016/j.electacta.2022.139871

[24] Tu J, Li H, Zhang J et al (2019) Latent heat and thermal conductivity enhancements in polyethylene glycol/polyethylene glycol-grafted graphene oxide composites. Adv Compos Hybrid Mater 2:471–480. https://doi.org/10.1007/s42114-019-00083-x

[25] Zhang H, Zhong J, Liu Z, Mai J, Liu H, Mai X (2021) Dyed bamboo composite materials with excellent anti-microbial corrosion. Adv Compos Hybrid Mater 4:294–305. https://doi.org/10.1007/s42114-020-00196-8

[26] Zhang M, Du H, Liu K et al (2021) Fabrication and applications of cellulose-based nanogenerators. Adv Compos Hybrid Mater 4:865–884. https://doi.org/10.1007/s42114-021-00312-2

[27] Zheng M, Wei Y, Ren J et al (2021) 2-aminopyridine functionalized magnetic core–shell Fe_3O_4@polypyrrole composite for removal of Mn (VII) from aqueous solution by double-layer adsorption. Sep Purif Technol 277:119455. https://doi.org/10.1016/j.seppur.2021.119455

[28] Zhu X, Zhang J, Zhou J et al (2021) Adsorption characteristics and conformational transition of polyethylene glycol–maleated rosin polyesters on the water–air surface. Adv Compos Hybrid Mater. https://doi.org/10.1007/s42114-021-00354-6

[29] Chang B, Li Y, Wang W et al (2021) Impacts of chain extenders on thermal property, degradation, and rheological performance of poly(butylene adipate-co-terephthalate). J Mater Res 36:3134–3144. https://doi.org/10.1557/s43578-021-00308-0

[30] Al-Itry R, Lamnawar K, Maazouz A (2012) Improvement of thermal stability, rheological and mechanical properties of PLA, PBAT and their blends by reactive extrusion with functionalized epoxy. Polym Degrad Stab 97:1898–1914. https://doi.org/10.1016/j.polymdegradstab.2012.06.028

[31] Malda J, Woodfield TBF, van der Vloodt F et al (2005) The effect of PEGT/PBT scaffold architecture on the composition of tissue engineered cartilage. Biomaterials 26:63–72. https://doi.org/10.1016/j.biomaterials.2004.02.046

[32] Platnieks O, Gaidukovs S, Thakur VK, Barkane A, Beluns S (2021) Bio-based poly (butylene succinate): recent progress, challenges and future opportunities. Eur Polym J. https://doi.org/10.1016/j.eurpolymj.2021.110855

[33] Qiu S, Zhou Y, Waterhouse GIN et al (2021) Optimizing interfacial adhesion in PBAT/PLA nanocomposite for biodegradable packaging films. Food Chem. https://doi.org/10.1016/j.foodchem.2020.127487

[34] Hayes DG, Wadsworth LC, Sintim HY et al (2017) Effect of diverse weathering conditions on the physicochemical properties of biodegradable plastic mulches. Polym Test 62:454–467. https://doi.org/10.1016/j.polymertesting.2017.07.027

[35] Rabnawaz M, Wyman I, Auras R, Cheng S (2017) A roadmap towards green packaging: the current status and future outlook for polyesters in the packaging industry. Green Chem 19:4737–4753. https://doi.org/10.1039/c7gc02521a

[36] Wang Y, Wang P, Du Z, Liu C, Shen C, Wang Y (2021) Electromagnetic interference shielding enhancement of poly(lactic acid)-based carbonaceous nanocomposites by poly(ethylene oxide)-assisted segregated structure: a comparative study of carbon nanotubes and graphene nanoplatelets. Adv Compos Hybrid Mater. https://doi.org/10.1007/s42114-021-00320-2

[37] Wei Y, Luo W, Li X et al (2022) PANI-MnO2 and Ti3C2Tx (MXene) as electrodes for high-performance flexible asymmetric supercapacitors. Electrochim Acta 406:139874. https://doi.org/10.1016/j.electacta.2022.139874

[38] Wei Y, Zheng M, Luo W et al (2022) All pseudocapacitive MXene-MnO2 flexible asymmetric supercapacitor. J Energy Storage 45:103715. https://doi.org/10.1016/j.est.2021.103715

[39] Cheng XQ, Li S, Bao H et al (2021) Poly(sodium-p-styrenesulfonate)-grafted UiO-66 composite membranes boosting highly efficient molecular separation for environmental remediation. Adv Compos Hybrid Mater 4:562–573. https://doi.org/10.1007/s42114-021-00253-w

[40] Iwata T (2015) Biodegradable and bio-based polymers: future prospects of eco-friendly plastics. Angew Chem Int Ed 54:3210–3215. https://doi.org/10.1002/anie.201410770

[41] Kivade SB, Gunge A, Nagamadhu M, Rajole S (2021) Mechanical and dynamic mechanical behavior of acetylation-treated plain woven banana reinforced biodegradable composites. Adv Compos Hybrid Mater. https://doi.org/10.1007/s42114-021-00247-8

[42] Ma Y, Zhuang Z, Ma M et al (2019) Solid polyaniline dendrites consisting of high aspect ratio branches self-assembled using sodium lauryl sulfonate as soft templates: synthesis and electrochemical performance. Polymers 182:121808. https://doi.org/10.1016/j.polymer.2019.121808

[43] Saratale GD, Jung M-Y, Oh M-K (2016) Reutilization of green liquor chemicals for pretreatment of whole rice waste biomass and its application to 2,3-butanediol production. Bioresour Technol 205:90–96. https://doi.org/10.1016/j.biortech.2016.01.028

[44] Wei Y, Luo W, Zhuang Z et al (2021) Fabrication of ternary MXene/MnO2/polyaniline nanostructure with good electrochemical performances. Adv Compos Hybrid Mater 4:1082–1091. https://doi.org/10.1007/s42114-021-00323-z

[45] Zhang J, Li J, Tang Y, Lin L, Long M (2015) Advances in catalytic production of bio-based polyester monomer 2,5-furandicarboxylic acid derived from lignocellulosic biomass. Carbohydr Polym 130:420–428. https://doi.org/10.1016/j.carbpol.2015.05.028

[46] Zhuang Z, Wang W, Wei Y, Li T, Ma M, Ma Y (2021) Preparation of polyaniline nanorods/manganese dioxide nanoflowers core/shell nanostructure and investigation of electrochemical performances. Adv Compos Hybrid Mater 4:938–945. https://doi.org/10.1007/s42114-021-00225-0

[47] Ouyang L, Huang W, Huang M, Qiu B (2022) Polyaniline improves granulation and stability of aerobic granular sludge. Adv Compos Hybrid Mater. https://doi.org/10.1007/s42114-022-00450-1

[48] Si Y, Li J, Cui B et al (2022) Janus phenol-formaldehyde resin and periodic mesoporous organic silica nanoadsorbent for the removal of heavy metal ions and organic dyes from polluted water. Adv Compos Hybrid Mater. https://doi.org/10.1007/s42114-022-00446-x

[49] Zhao Z, Zhao R, Bai P et al (2022) AZ91 alloy nanocomposites reinforced with Mg-coated graphene: Phases distribution, interfacial microstructure, and property analysis. J Alloys Compd. https://doi.org/10.1016/j.jallcom.2021.163484

[50] Li Z, Li Y, Lei H et al (2022) The effect of synergistic/inhibitory mechanism of terephthalic acid and glycerol on the puncture, tearing, and degradation properties of PBSeT copolyesters. Adv Compos Hybrid Mater. https://doi.org/10.1007/s42114-021-00405-y

[51] Yu S, Cui J, Wang X, Zhong C, Li Y, Yao J (2020) Preparation of sebacic acid via alkali fusion of castor oil and its several derivatives. J Am Oil Chem Soc 97:663–670. https://doi.org/10.1002/aocs.12342

[52] Moreau C, Belgacem MN, Gandini A (2004) Recent catalytic advances in the chemistry of substituted furans from carbohydrates and in the ensuing. Polym Chem. https://doi.org/10.1002/chin.200431251

[53] Papageorgiou GZ, Papageorgiou DG, Terzopoulou Z, Bikiaris DN (2016) Production of bio-based 2,5-furan dicarboxylate polyesters: Recent progress and critical aspects in their synthesis and thermal properties. Eur Polym J 83:202–229. https://doi.org/10.1016/j.eurpolymj.2016.08.004

[54] Burgess SK, Leisen JE, Kraftschik BE, Mubarak CR, Kriegel RM, Koros WJ (2014) Chain mobility, thermal, and mechanical properties of poly(ethylene furanoate) compared to poly(ethylene terephthalate). Macromolecules 47:1383–1391. https://doi.org/10.1021/ma5000199

[55] Zhu J, Cai J, Xie W et al (2013) Poly(butylene 2,5-furan dicarboxylate), a biobased alternative to PBT: synthesis, physical properties, and crystal structure. Macromolecules 46:796–804. https://doi.org/10.1021/ma3023298

[56] Burgess SK, Mikkilineni DS, Yu DB et al (2014) Water sorption in poly(ethylene furanoate) compared to poly(-ethylene terephthalate). Part 2: Kinetic sorption. Polymers 55:6870–6882. https://doi.org/10.1016/j.polymer.2014.10.065

[57] Papageorgiou GZ, Tsanaktsis V, Bikiaris DN (2014) Synthesis of poly(ethylene furandicarboxylate) polyester using monomers derived from renewable resources: thermal behavior comparison with PET and PEN. Phys Chem Chem Phys 16:7946–7958. https://doi.org/10.1039/c4cp00518j

[58] Wang J, Liu X, Jia Z, Sun L, Zhang Y, Zhu J (2018) Modification of poly(ethylene 2,5-furandicarboxylate) (PEF) with 1,4-cyclohexanedimethanol: influence of stereochemistry of 1,4-cyclohexylene units. Polymers 137:173–185. https://doi.org/10.1016/j.polymer.2018.01.021

[59] Wang J, Liu X, Zhang Y, Liu F, Zhu J (2016) Modification of poly(ethylene 2,5-furandicarboxylate) with 1,4-

cyclohexanedimethylene: Influence of composition on mechanical and barrier properties. Polymers 103:1–8. https://doi.org/10.1016/j.polymer.2016.09.030

[60] Wang J, Liu X, Zhu J, Jiang Y (2017) Copolyesters based on 2,5-Furandicarboxylic Acid (FDCA): effect of 2,2,4,4-tetramethyl-1,3-cyclobutanediol units on their properties. Polymers. https://doi.org/10.3390/polym9090305

[61] Ma J, Yu X, Xu J, Pang Y (2012) Synthesis and crystallinity of poly(butylene 2,5-furandicarboxylate). Polymer 53:4145–4151. https://doi.org/10.1016/j.polym.2012.07.022

[62] Hu H, Zhang R, Shi L, Ying WB, Wang J, Zhu J (2018) Modification of poly(butylene 2,5-furandicarboxylate) with lactic acid for biodegradable copolyesters with good mechanical and barrier properties. Ind Eng Chem Res 57:11020–11030. https://doi.org/10.1021/acs.iecr.8b02169

[63] Hu H, Zhang R, Wang J, Ying WB, Zhu J (2018) Fully biobased poly(propylene succinate-co-propylene furandicarboxylate) copolyesters with proper mechanical, degradation and barrier properties for green packaging applications. Eur Polym J 102:101–110. https://doi.org/10.1016/j.eurpolymj.2018.03.009

[64] Papageorgiou GZ, Papageorgiou DG, Tsanaktsis V, Bikiaris DN (2015) Synthesis of the bio-based polyester poly(propylene 2,5-furan dicarboxylate). Comparison of thermal behavior and solid state structure with its terephthalate and naphthalate homologues. Polymers 62:28–38. https://doi.org/10.1016/j.polymer.2015.01.080

[65] Vannini M, Marchese P, Celli A, Lorenzetti C (2015) Fully biobased poly(propylene 2,5-furandicarboxylate) for packaging applications: excellent barrier properties as a function of crystallinity. Green Chem 17:4162–4166. https://doi.org/10.1039/c5gc00991j

[66] Yang Z, Peng H, Wang W, Liu T (2010) Crystallization behavior of poly(ε-caprolactone)/layered double hydroxide nanocomposites. J App Polym Sci 116:2658–2667. https://doi.org/10.1002/app.31787

[67] Li Z, Li Y, Dong X et al (2021) Synthesis, characterization and properties of poly(butanediol sebacate-butanediol terephthalate) (PBSeT) copolyesters using glycerol as cross-linking agent. Mater Today Commun. https://doi.org/10.1016/j.mtcomm.2021.102557

[68] Heidarzadeh N, del Valle LJ, Franco L, Puiggali J (2020) Improvement of biodegradability and biocompatibility of electrospun scaffolds of poly(butylene terephthalate) by incorporation of sebacate units. Macromol Res 28:23–32. https://doi.org/10.1007/s13233-020-8009-0

[69] Lu J, Wu L, Li B-G (2017) High molecular weight polyesters derived from biobased 1,5-pentanediol and a variety of aliphatic diacids: synthesis, characterization, and thermomechanical properties. ACS Sustain Chem Eng 5:6159–6166. https://doi.org/10.1021/acssuschemeng.7b01050

[70] Xie H, Wu L, Li B-G, Dubois P (2018) Poly(ethylene 2,5-furandicarboxylate-mb-poly(tetramethylene glycol)) multiblock copolymers: from high tough thermoplastics to elastomers. Polymers 155:89–98. https://doi.org/10.1016/j.polymer.2018.09.033

[71] Konstantopoulou M, Terzopoulou Z, Nerantzaki M et al (2017) Poly(ethylene furanoate-co-ethylene terephthalate) biobased copolymers: synthesis, thermal properties and cocrystallization behavior. Eur Polym J 89:349–366. https://doi.org/10.1016/j.eurpolymj.2017.02.037

[72] Huang F, Wu L, Li B-G (2020) Sulfonated biodegradable PBAT copolyesters with improved gas barrier properties and excellent water dispersibility: from synthesis to structure-property. Polym Degrad Stab. https://doi.org/10.1016/j.polymdegradstab.2020.109391